Structure and evolution of intense austral cut-off lows

Article

Accepted Version

Pinheiro, H., Gan, M. and Hodges, K. ORCID: https://orcid.org/0000-0003-0894-229X (2021) Structure and evolution of intense austral cut-off lows. Quarterly Journal of the Royal Meteorological Society, 147 (743). pp. 1-20. ISSN 1477-870X doi: 10.1002/qj.3900 Available at https://centaur.reading.ac.uk/91776/

To link to this article DOI: http://dx.doi.org/10.1002/qj.3900

Publisher: Royal Meteorological Society

Structure and evolution of intense austral Cut-off Lows

Henri Pinheiro[1], Manoel Gan[1], and Kevin Hodges[2]

[1]Center for Weather Forecast and Climate Studies, National Institute for Space Research, Sao Jose dos Campos, SP, Brazil

[2]Department of Meteorology, The University of Reading, Reading, United Kingdom

Corresponding author: henrirpinheiro@gmail.com

Telephone Number: +55 12 3208-6000

ORCID: 0000-0003-4363-3206

ABSTRACT

This study examines the three-dimensional structure and evolution of the 200 most intense Cut-off Lows (COLs) in the Southern Hemisphere (SH). This is done using feature tracking and cyclone-centred compositing based on the ERA-Interim reanalysis. Composites confirm the existence of a well-defined tropospheric moist cold core co-located with warm dry air in the lower stratosphere. Such cores are surrounded by regions of strong temperature gradients (frontal zones) which move downstream throughout the life cycle. The stratospheric air intrusion into the troposphere is identified in vertical cross-sections of potential vorticity and ozone, a process referred to as tropopause folding. Precipitation occurs ahead of the COLs because of the low (high)-level convergence (divergence) and strong upward motion. The maximum precipitation is observed during decay, indicating a possible link between COLs and surface cyclones. Composites conditioned on relative vorticity and precipitable water suggest these variables may be related to precipitation. The COLs exhibit a westward tilt during their early stages but they change to a barotropic state in the mature stage. Finally, the main characteristics of the COLs are summarized by categories which discriminate different intensities, indicating there are differences in the structure of COLs with consequences for precipitation. These efforts aim to provide new insights into the development of COLs in the SH which could aid in identifying and forecasting their various types and associated precipitation patterns.

Keywords: Cut-off Lows; Composites, Structure; Life Cycle, Southern Hemisphere.

1 Introduction

Cut-off Low (COL) pressure systems are upper-tropospheric cold lows that form when a mid-latitude upper-tropospheric trough deepens equatorward (Palmén 1949; Palmén and Newton 1969). Typical COLs are short-lived and quasi-stationary systems with irregular trajectories, thereby posing a great challenge for their prediction even with modern forecasting systems (Bozkurt et al. 2016; Muofhe et al. 2020). The statistics of COLs such as their mean preferred locations are extensively documented in studies for the Northern Hemisphere (NH, Price and Vaughan 1992; Nieto et al. 2005; 2008) and Southern Hemisphere (SH; Fuenzalida et al. 2005; Reboita et al. 2010; Pinheiro et al. 2017). Other studies have investigated the key structural features of COLs (Palmén 1949; Hoskins et al. 1985; Qi et al. 1999; Garreaud and Fuenzalida 2007; Satyamurty and Seluchi 2007; Godoy et al. 2011; Ndarana et al. 2020) but have focused on specific regions or individual events, which may be subject to uncertainty due to the system variability. Therefore, the average characteristics related to the structure and evolution of COLs have had less attention, in particular in the SH.

There are many reasons why it is important to study COLs, one of which is related to precipitation and its impact on human activities. For example, COLs are associated with heavy rainfall events and severe flooding in southern Europe and northern Africa (Knippertz and Martin 2005; Delgado et al. 2007; Llasat et al. 2007; Nieto et al. 2008). In the Southern Hemisphere, COLs are found to account for about half of the total precipitation in southeast Australia (Pook et al. 2006), producing more of the heavier rainfall and flood events in coastal areas (Risbey et al. 2009). They are often associated with heavy precipitation on the Eastern Cape coast (South Africa; Singleton and Reason 2006) and anomalously high precipitation may occasionally occur in arid regions, as observed in the Namib and Kalahari Deserts in southern Africa (Muller et al. 2008) and the Atacama Desert in South America (Bozkurt et al. 2016; Reboita and Veiga 2017). Additionally, COLs play an important role in the stratosphere-troposphere exchange (STE) (Price and Vaughan 1993), which can occasionally result in abrupt changes in the ozone concentration at high elevation locations (Rondanelli et al. 2002).

Early studies have documented how COLs present well-defined and asymmetrical cloud and precipitation structures where deep convective clouds are typically located on the eastern edge of the vortex, contrasting with relatively dry air on the upstream side (Griffiths et al. 1998; Singleton and Reason 2006; Satyamurty and Seluchi 2007). However, other studies have shown that convective clouds can be seen to the west of the vortex for COLs in the Mediterranean Region (Delgado et al. 2007; Nieto et al. 2008), suggesting there may be regional differences regarding the cloud and precipitation patterns or there are differences in how COLs are defined in each region and study. Differences in precipitation are also evident with respect to the lifecycle stage. Although Delgado et al. (2007) showed that the probability of heavy precipitation decreases considerably after the peak intensity in the Mediterranean COLs, other studies have demonstrated that most of the precipitation in COLs that affect South America occur from the mature to the decay stages (Satyamurty and Seluchi 2007; Godoy et al. 2011; Bozkurt et al. 2016).

Some of the characteristics of COLs that occur in the NH, but particularly in the Iberian Peninsula and Mediterranean regions, were identified and conceptualized by Nieto et al. (2005) and Llasat et al. (2007). The study of Nieto et al. (2005) proposed a conceptual model of COLs that involves four stages: the upper-level trough, tear-off, cut-off and final stage. These stages represent an idealized view of how key meteorological fields vary through the COL lifecycle. However, this structural model appears not to address some crucial aspects, such as the precipitation and how it varies at each stage. It is also unknown if the Nieto's conceptual model is relevant for COLs in the SH. Hence, a more comprehensive analysis of these systems is needed.

The understanding of the structure and evolution of COLs is one of the keys to understand their associated cloud and precipitation features. There have been several studies focusing on mid-upper level COLs in both hemispheres, but the literature is limited concerning the vertical structure of COLs and its relation with impacts such as precipitation. Scherhag (1939) stated that COLs are strictly related to depressions at high levels with no surface cyclone. Indeed, COLs are stronger in the upper troposphere and weaken toward the surface, and it is not uncommon to find an anti-cyclonic circulation at low levels (Kuo 1949). However, there are situations in which the vortex deepens downward, leading to surface cyclogenesis (Gan and Rao 1996; Mikyfunatsu 2004). Thus it is plausible that the vertical depth (extent) is highly variable in COLs and crucial to determining the cloud and precipitation properties, as earlier suggested by Frank (1970) and demonstrated by the findings of Porcù et al. (2007). Porcù et al. (2007) found that deep COLs in the Mediterranean Region are associated with high rainfall rates affecting relatively large areas, while shallow COLs (defined as the vortices confined to high levels) do not often produce precipitation.

There have been several regional case studies investigating the structure of COLs (Palmén 1949; Hoskins et al. 1985; Price and Vaughan 1993; Satyamurty and Seluchi 2007; Godoy et al. 2011). The pioneering study of Palmén (1949) showed that COLs have a quasi-barotropic structure with a symmetric circulation at high levels, where maximum winds occur at about 200 hPa and intersect with the tropopause region. Other studies have described the structural key features using observations derived from reanalysis datasets (Mikyfunatsu 2004; Nieto et al. 2008; Ndarana et al. 2020) or numerical model outputs (Garreaud and Fuenzalida 2007; Bozkurt et al. 2016). Several studies have used Potential Vorticity (PV) as a tool to identify and analyse the dynamical evolution of COLs and the tropopause folding. This process contributes to the transfer of high-PV air from the polar stratospheric reservoir to the subtropical troposphere. There are numerous case studies (Palmén 1949; Hoskins et al., 1985; Bell and Bosart 1993) describing the thermal structural properties of COLs, showing the presence of a well-defined cold core in the middle and upper troposphere with a stratospheric warm core aloft. This characteristic contributes to increased atmospheric instability, particularly if the system moves over warm moist surfaces (Kousky and Gan 1981; Nieto et al. 2005).

It is well-known that COLs are characterised by strong baroclinicity in the upper layers of the troposphere, as documented in several studies (Palmén 1949; Shapiro 1970; Hoskins 1971). An attempt to identify the baroclinic zones associated with the COLs that occur in the Mediterranean region was carried out by Sabo (1992). The study of Sabo (1992) used the thermal frontal parameter (TFP; Clarke and Renard 1966) and found the existence of two baroclinic zones, one in front of the COL centre (i.e. east of the geopotential minimum) which is connected with the frontal cloud band, and the other behind the COL centre associated with a baroclinic boundary. More recently, Nieto et al. (2005) used the TFP as a conceptual criterion for identifying COLs in the NH (see step 3 of their methodology). According to these studies, the main baroclinic zone is typically found downstream of the trough axis, where the TFP values are higher than those located in the COL centre.

Most conceptual models and theories of COLs have essentially been developed through case studies (Palmén 1949; Hoskins et al. 1985; Nieto et al. 2005; Llasat et al. 2007), providing a valuable framework to understand the dynamical evolution of COLs. However, limited sample sizes may bias the conceptual models to specific cases. Hence, basing a conceptual model on a larger sample size may provide improved insights into COL behaviour. ~~Since most~~Most conceptual models have been built on evidence-based case studies for COLs in the NH, where their properties may differ from those associated with SH COLs ~~(~~because of the association with the zonal asymmetries in topography, land-sea contrast, and seasonal variation of jet stream~~)~~.~~ and motivated~~ Motivated by the limited number of studies on the structure of COLs in the SH, and hypothesizing that SH COLs may be different from NH COLs, it is therefore important to identify the average properties presented by typical austral COLs that may be considered as features in conceptual models of SH COLs.

The aim of this study is to provide a comprehensive analysis of the mean structure and evolution of the typical COLs observed in the SH. A compositing methodology is used to analyse the key features of COLs through horizontal and vertical composites of several fields relevant to the structure of COLs. Given the differences in the COL characteristics observed from case to case, the main questions to be addressed in this study are the following:

1) What is the typical structure and lifecycle of SH subtropical COLs?
2) How is the precipitation related to the magnitude of moisture and intensity of the COLs observed in the SH?

The focus of this paper is on the extreme austral COLs obtained as the 200 most intense systems (> 98th percentile) identified in reanalysis data during a 36-year period (1979-2014). This analysis goes beyond the scope of earlier studies, making results more statistically robust and providing a guiding framework for the development of conceptual models for COLs.

The methods used to track and create composite fields of COLs are described in Section 2. The spatial statistics for all COLs and the strongest COLs are presented in Section 3. In Section 4 we describe the main structural features of COLs through horizontal and vertical composite fields and provide further insights into the COL structure in the Supplementary Material. Section 5 focuses on the composites of the life cycle of COLs. Section 6 examines how precipitation varies with respect to the intensity of COLs and their moisture content. Finally, two conceptual models are proposed in Section 7 to explain the effect of the intensity on the vertical structure of COLs and their precipitation, together with discussion of the results and concluding remarks.

2 Data and analysis methodologies

2.1 ERA-Interim Reanalysis

The main data used in this study comes from the European Centre for Medium-Range Weather Forecast (ECMWF) ERA-Interim (ERAI) Reanalysis (Dee et al. 2011), which is used to provide a detailed view of the structure and evolution of SH COLs. In the absence of any truth to compare with, this reanalysis is in good agreement with other contemporary reanalyses in respect of COL identification and distribution in the SH (Pinheiro et al. 2020). ERAI has been produced by ECMWF using a spectral model with TL255 horizontal resolution (~80 km) and 60 vertical hybrid levels with the model top at 0.1 hPa. A 4D-Var data assimilation scheme is used to assimilate the diverse observations from satellite and terrestrial data. For the surface boundary conditions, the Sea Surface Temperature (SST) and Sea Ice Concentration (SIC) are prescribed using different SST and SIC products, as described in Dee et al. (2011). The ERAI data was used for the period from 1979 to 2014.

2.2 Tracking and compositing methodology

The SH COLs are identified and tracked in two fields (6 hourly) independently as features with minima below -1.0 x 10^{-5} s^{-1} for filtered 300-hPa relative vorticity (ξ_{300}) and -50 geopotential meters (gpm) for filtered 300-hPa geopotential anomaly (Z'_{300}). The Z'_{300} is obtained by removing the zonal mean from geopotential data (Z_{300}) in order to facilitate the identification (Pinheiro et al. 2019). The reason for the use of both ξ_{300} and Z'_{300} is to give a generic view of the structure of the SH COLs. Before the identification and tracking, the data are spectrally truncated to T42 for vorticity, as this is a very noisy field, and T63 for geopotential which is a smoother field. The respective minima are first identified at each time step on the grid and then refined using an interpolation and minimization method (Hodges, 1995). The tracking is performed by first initializing a set of tracks from the identified 'feature points' using a nearest neighbour approach and then applying an optimization of a cost function for track smoothness which is subject to adaptative constraints appropriate to the type of motion for the COLs, as discussed in Pinheiro et al. (2019). A post tracking filtering with respect to the 300-hPa horizontal wind components (U_{300}, V_{300}) is used to avoid open troughs in the analysis. Four offset points located at 5^{o} (geodesic distance) from the tracked minima are sampled along the tracks in four directions relative to the centre, which are 0° ($U_{300}> 0$), 90° ($V_{300}<0$), 180° ($U_{300}<0$), and 270° ($V_{300}> 0$) relative to North. Given the different choice of methods derived from different variable combinations, the method described above has been found effective for COL identification (Pinheiro et al. 2019) as the mentioned scheme detects the largest number of COLs generally seen in geopotential maps. Only the tracks that reach 40^{o}S or have their genesis north of 40^{o}S and last at least 24h are included. To discard tropical systems, tracks that occur north of 15^{o}S are excluded.

A compositing methodology that has previously been applied to tropical and extratropical cyclones (Bengtsson et al. 2009; Catto et al. 2010; Dacre et al. 2012; Hawcroft et al. 2016) is applied here to obtain the composite structure and evolution of COLs. The focus is on extreme COLs obtained from the 200 most intense systems that can be found in both ξ_{300} and Z'_{300}. The identically same COLs are identified by matching the tracks from the vorticity and geopotential that have a mean separation distances less than four degrees and that overlap in time by at least 50% of their track points. For the composite procedure, each COL is centred on the time when the ξ_{300} ~~and~~ ~~Z'_{300}~~ lowest minimum~~a~~ ~~are~~is found along each track. Then, single level fields (such as precipitation) or multi-level fields (such as winds) are extracted on to a radial grid with maximum radius of 15º centred on the COL centres (15 degree ~ 1500 km), which is suitable for capturing the synoptic features of COLs. Since COLs move preferentially eastward and we aim to examine the horizontal tilt, composites are not rotated to the direction of propagation prior to compositing (Catto et al. 2010). This allows us to view the COL horizontal tilt during its development referred to cardinal points relative to North (0º). The vertical tilt is obtained as the (geodesic) angle between the ξ_{300} tracked minima and the corresponding vorticity minima at a number of levels from 300 hPa down to 1000 hPa, similar to that performed by Bengtsson et al. (2009) for extratropical cyclones except the search is performed downwards.

3 Spatial statistics for all and the strongest Cut-off Lows

Before presenting the results for the structure and evolution of COLs, the hemispheric COL climatology is shown in Figure 1 as the track density computed using spherical kernel estimators (Hodges 1996) using all identified matched COLs (total number is 11,542 tracks) and for the 200 most intense COLs that match for a 36-year period. The climatological track density shows a distribution very similar to that obtained in earlier studies of mid-upper level COLs (Fuenzalida et al. 2005; Reboita et al. 2010; Ndarana and Waugh 2010; Favre et al. 2012; Pinheiro et al. 2017) where the highest values are found in the vicinity of the continents. For the strongest COLs, in particular, the track density maxima shift to more poleward latitudes, being located on the poleward side of the main region of the track density. This is the case for the strongest COLs located in the eastern Indian Ocean, southeast Australia, and southern Africa, where values exceed 0.3 units, coinciding with the location of large values of mean intensity of COLs (see Fig. 5 of Pinheiro et al. 2017). The strongest COLs that are located at more equatorward latitudes in the SH occur off the west coast of South America (values up to 0.4) where such events frequently affect areas of northern Chile and southern Peru (Garreaud and Fuenzalida 2007; Bozkurt et al. 2016; Reyers and Shao 2019). However, in the western Pacific where the climatological track density is relatively large, the frequency for the strongest COLs is quite small. In this sector, the high COL activity is partly associated with the high-frequency of blocking (Trenberth and Mo 1985; Marques and Rao 2000) which may differ from the structure of typical COLs, as described by Palmén (1949). According to Hoskins et al. (1985), many COLs can develop in association with blocking highs as part of the same phenomenon, which can be distinguished by the sign of the isentropic PV anomaly.

4 Composites of Cut-off Low structure

The main synoptic-scale features of COLs that have been described in case studies and conceptual models are compared with the composites of the 200 most intense COLs from the ERAI reanalysis. The structure of COLs is described through different variables and pressure levels using the identical systems identified in both ξ_{300} and Z'_{300}. Although the analysis is based on the ξ_{300} and Z'_{300} COLs, composites are extracted from the time of maximum intensity in ξ_{300} for each COL (see Fig.1 for the locations of the maximum intensity in each COL), so the discussion will be in terms of the relative vorticity. The upper-level features of SH COLs will be presented in Section 4.1, followed by an examination of the vertical features in Section 4.2.

4.1 Upper-level features

In this section the key upper-level features of the strongest COLs are examined at maximum intensity (lowest minima) through different horizontal fields. The composite of the zonal component of the 300-hPa wind speed (Fig. 2a) exhibits a north-south asymmetry where the highest values occur to the north/northeast (wind speeds reaching 50 m/s) as a result of meridional divergence of vorticity advection (Ndarana et al. 2020), contrasting with relatively low easterly winds to the south associated with the vortex detachment. According to Ndarana et al. (2020), the vorticity advection convergence decelerates the flow and facilitates the formation of a split jet structure. The meridional wind component (Fig. 2b) demonstrates there is much more symmetry with respect to the west-east direction with maximum values ranging from 40 to 50 m/s. The spatial pattern of the absolute wind speed shows two maxima with a discrete westward tilt: the stronger centre occurs in the top right-hand quadrant of the composite COL (northeastern sector); the other centre is located to the west of the COL centre with a smaller extent than the former. However, the wind speed near the tropopause varies widely with the life cycle (see Fig. 5) due to the kinetic energy which is dispersed from upstream by the ageostrophic flux (Gan and Piva 2013). A prominent feature of the COLs is their high-PV anomaly (Fig. 2a-b) which stretches into a narrow streamer equatorward and becomes an isolated PV contour. This process is associated with tropopause folds and downward transport of ozone (see Fig. S2 in the Supplementary Material).One of the main distinguishing features of COLs described in previous conceptual models (Nieto et al. 2005; Llasat et al. 2007) is the cold air in the mid-upper troposphere. Some studies described in the literature have shown that the cold air associated with a COL is superimposed on warmer air in the lower stratosphere, characterising a thermal dipole pattern (Palmén 1949; Griffiths et al. 1998; Campetella and Possia 2007; Satyamurty and Seluchi 2007). To identify the approximate position of the cold and warm cores within COLs, the zonal temperature anomaly was examined at different pressure levels (not shown), this suggests that the cold (warm) anomalies cover a deep layer in the troposphere (stratosphere). Figure 2c-d shows the anomalous temperature and TFP (Clarke and Renard 1966) at 400 and 200 hPa which are the two closest levels to the upper-level COLs that can ideally be identified as the cold and warm regions, respectively. It is apparent that the horizontal location of the tropospheric cold anomalies coincides fairly well with that of the stratospheric warm anomalies above. The TFP is used here to identify the baroclinic zones within the COLs since it takes into account the changes of temperature in the direction of the temperature gradient. This exhibits the maxima in the top left-hand quadrant for the composites, with cold and warm cores associated with correspondingly strong horizontal temperature gradients. We found similar results using earlier lifecycle stages, whereas in the decaying lifecycle stage the maximum TFP occurs on the downstream side of the COL as shown in the supplementary material (Sections 2 and 5). This is in agreement with the conceptual model of Keyser and Shapiro (1986), where the frontal zones propagate downstream throughout the lifecycle of upper-level eddies. However, there are significant differences from case to case which is smoothed out by the compositing. The standard deviation of TFP (Figures S5 and S6 in the Supplementary Material) shows significant spread which can be attributed to different development scenarios.

4.2 Vertical features

We now look at the vertical structure of the composite COLs at maximum intensity for several fields through the West-East (W-E) and South-North (S-N) cross sections. The 15^o spherical cap region is extracted for ten pressure levels from 1000 hPa up to 100 hPa using the track point at 300 hPa as the reference. Thus, the vertical tilt of COLs is not taken into account for this specific analysis, but it will be examined later. Vertical composites can be produced using either the vorticity or geopotential minimum at each pressure level to extract the region centred on the minimum referred to each level, but the results are not changed since tilt is minor in the mature stage. The vertical composites are exhibited within a 12^o radius, which is where the synoptic-scale processes dominate. Composites are also produced at a specified offset time relative to the time of maximum intensity of COLs identified in both ξ_{300} and Z'_{300}, and are discussed later in Section 5.

Parameters such as wind speed, geopotential, relative vorticity and PV are conveniently discussed together in order to highlight the typical dynamic structure of COLs. A nearly zonally-symmetric circulation is seen in the middle and upper troposphere for the W-E cross section (Fig. 3a) where the centres of maximum wind speed are located between 300 and 200 hPa and about 4^o-6^o west and east of the COL centre, with the eastern centre a little stronger and higher than the western centre. The magnitude of the winds is greatly reduced horizontally and vertically away from the maxima, indicating a region of strong horizontal and vertical wind shear in the upper troposphere. However, the S-N cross section (Fig. 3b) shows an asymmetric circulation with rather strong winds at 250 hPa in the northern part of the COL, associated with the westerly winds, which is consistent with Fig. 2a. Similar results have been observed for a COL in North America by the pioneering study of Palmén (1949), which attributed the asymmetry of the N-S cross section to a lack of observations in the southern United States and Mexico. Further studies such as Hsieh (1949) and Kelley and Mock (1982) confirmed the asymmetry does exist with stronger winds on the equatorward side of the COL. The results of our study are consistent with previous findings as the relatively weak winds appear on the poleward side of the COL and occur due to the weakening of westerlies and reversal of winds associated with the cut-off process.

The full resolution of relative vorticity and geopotential height anomaly (Figure 3a-b) are examined to demonstrate the vertical structure of COLs in terms of intensity. The maximum intensity occurs near the tropopause where the wind (shear) magnitude is maximum, but the values gradually weaken toward the surface, though cyclonic features are still found in the lower troposphere. It can be seen that the largest geopotential anomalies (values lower than -250 gpm) coincide in location with the vorticity minimum ($-25.0 \times 10^{-5}\ s^{-1}$) in the W-E cross section, but the geopotential minimum is slightly offset from the vorticity minimum in the S-N cross section due to the shear component effect in the upper-level flow (Bell and Keyser 1993). Similar results are obtained if the compositing were performed referencing to the 500-hPa vorticity COLs (not shown). This means the maximum intensity of COLs is expected to be at about 300 hPa even if the tracking were performed at a level other than 300 hPa. In general, our results are consistent with previous studies on COLs in subtropical regions, indicating that COLs have the strongest intensities at about the 300 hPa level (Quispe and Avalos 2006; Satyamurty and Seluchi 2007). This is different from other types of tropopause vortices such as tropopause tropical vortices (TTV) which have maximum intensities at higher levels (Kousky and Gan 1981; Kelley and Mock 1982) or tropopause polar vortices (TPV, Cavallo and Hakim 2010) which have maximum intensities at lower levels.

Another typical aspect of COLs is the stratosphere-troposphere exchange as a consequence of the tropopause folding, as indicated by the 2.0 PVU surface (1 PVU = 10^{-6} m^2 s^{-1} K kg^{-1}) in Figure 3a-b. As the tropopause is lowered, high-PV stratospheric air is drawn down into the troposphere, leading to the formation of isolated stratospheric air cut-off from its origin, the so-called “stratospheric reservoir”. This process is often associated with Rossby wave breaking (RWB) events, which in turn are strongly connected to the PV deformation, as discussed in many studies (Hoskins et al. 1985; Wernli and Sprenger 2007; Ndarana and Waugh 2010). The deepest intrusion of PV occurs when the COLs reach their maximum intensity, particularly for the S-N cross section where an abrupt variation is observed on the equatorial side of the COL. For very intense COLs, the tropopause can reach lower levels (e.g. 600 hPa) as seen in Hoskins et al. (1985) and the Supplementary Material (Fig. S11a). Another consequence of the tropopause folding is the penetration of stratospheric ozone into the troposphere, as similarly observed in mid-latitude cyclones (Knowland et al. 2015). Composites show a clear tongue of ozone rich-air near the COL centre, similar to the PV distribution though the tropopause ozone fold in the COL centre is less pronounced compared to that in the PV. The vertical profile of ozone in COLs is given in the Supplementary Material (Section 2).

In Section 4.1, the TFP was used to identify the frontal zones within COLs which are located near the maximum temperature gradients. Here the vertical cross-section of the TFP (Fig. 3c-d) indicates that the baroclinic zones associated with COLs are not restricted to a narrow vertical band but they extend through a deep layer in the atmosphere. Frontal boundaries are clearly seen on the edges of the cold and warm cores in the W-E cross section where the narrow regions between the maximum and minimum TFP denote the largest temperature gradient. In the S-N cross section, a single well-defined maximum is found on the northern side of the COL which is consistent with the observed TFP distribution shown in Figure 2c-d.

The thermal structure of COLs is also examined in terms of isentropes and isotherms and is shown in Figure 4a-b. In the W-E cross section, the isentropes and isotherms appear to be almost completely symmetric, but the S-N cross section exhibits a discernible asymmetry. The tropospheric cold-core is apparent through the isotherms folding in the COL centre where it is surrounded by warmer air, while the stratospheric warm-core is marked by cooler temperatures in the vortex periphery, which is consistent with Figure 2c-d. Contrary to the temperature profile, the potential temperature increases with height, thus the cold core is depicted by a reversal of the lapse rate in the lower troposphere. The thermal structure represented in the composites agrees fairly well with previous studies (Palmén 1949; Griffiths et al. 1998; Campetella and Possia 2007; Satyamurty and Seluchi 2007) though the discontinuity of (potential) temperature typically seen along the tropopause is smoothed out by the compositing process.

The relative humidity anomaly (Fig. 4a-b) exhibits a pattern similar to the temperature anomaly but with opposite sign, where an anomalously dry stratospheric air is located above the moist tropospheric air. This pattern increases the relative humidity gradient across the tropopause which may be important to intensify the vortex circulation through radiative cooling, as observed in TPVs (Cavallo and Hakim 2010). The W-E cross section (Fig. 4a) shows that the moisture anomalies slope upward and eastward, while the S-N cross section (Fig. 4b) indicates a downward intrusion of stratospheric dry air into the northern flank of the COLs, which is coherent with the tropopause fold indicated by the 2.0 PVU (Fig. 3b).

The analysis of the three-dimensional structure of COLs continues by assessing other parameters such as the vertical velocity and divergence (Fig. 4c-d). Similar to the results discussed above, the largest contrasts are seen in the W-E cross section (Fig. 4c) since COLs move preferentially eastward as discussed before. This shows that the lower and middle troposphere are dominated by convergence downstream and divergence upstream of the storm centre, and the opposite holds at higher levels. As a consequence of the convergence at low levels, the maximum uplift takes place on the downstream side of COLs at 500-400 hPa (~5^o from the vortex centre) so that the moist air is transported to higher levels by the ascent. On the upstream side, a strong descending branch prevails with vertical velocity values comparable to the ascent region. It is apparent that the ascent and descent regions influence almost the entire troposphere, but the maximum values occur at the level of non-divergence, which is approximately at 500 hPa for the descent and somewhat higher for the ascent.

Given the characteristics described above, cloud formation and precipitation are expected to be present (absent) on the downstream (upstream) side of COLs. Also, the western side of a COL is associated with descent and stratospheric intrusions as the result of ageostrophic flow (Kentarchos et al. 1999). The results for the vertical structure of COLs are in close agreement with earlier studies (Mikyfunatsu et al. 2004; Knippertz and Martins 2005; Godoy et al. 2011), and the circulation features are even comparable to those found in TPVs (Cavallo and Hakim 2010), but may differ in TTVs which present cold air descending near the centre and warmer air rising at the periphery (Kousky and Gan 1981).

5 Composites of Cut-off Low lifecycle

This section focuses on the life cycle of COLs by compositing particular fields offset from the time of maximum intensity. This allows us to verify what occurs before and after the time when COLs reach their maximum intensity, namely, time zero. Several composite fields based on the most intense COLs are produced for different stages of the COL lifecycle (Figure 5) and discussed on the basis of the four stages described in the conceptual model of Nieto et al. (2005; 2008) outlined below, supplemented by the results from this study with the focus on the precipitation:

a. Upper-level trough (-48h): the initial stage starts from a cold, mid-latitude upper-tropospheric trough that deepens and tilts westward. This amplifying synoptic wave is associated with a band of precipitation orientated northwest-southeast that looks like a cold-frontal structure. Most of precipitation does not exceed the rainfall rate of 2.0 mm/6h.
b. Tear-off (-24h): as the trough deepens equatorward, the northern part of the wave detaches from the westerlies, leading to the formation of an isolated cyclonic vortex. Simultaneously, the band of precipitation gradually rotates cyclonically taking on a comma shape typical of extratropical cyclones. Maximum precipitation values increase to 2-3 mm/6h.
c. Cut-off and mature stages (0 and +24): the vortex becomes completely detached from the westerlies as COLs reach their maximum intensity. The intensification can be seen through the increased geopotential gradient and vertical motions. The precipitation rapidly increases during this stage, reaching the peak about 24h after the maximum intensity (maximum values are greater than 6.0 mm/6h). The increased precipitation is partly due to the strengthening of the ascent in response to the upper-level divergence just ahead of the system. This occurs when the divergence region superimposes the ascent region. Convective clouds are likely to develop in the vortex centre when the system passes over warm moist surfaces (Kousky and Gan 1981; Nieto et al. 2008) which leads to an increase in surface-based instability.

d. Decay (+48h): the decaying stage is characterised by a horizontal eastward tilt and a significant warming of the vortex core and surroundings before the vortex dissipates through diabatic effects as suggested by previous studies (Hoskins et al. 1985; Price and Vaughan 1993; Satyamurty and Seluchi 2007) or merges into the large-scale upper-level flow (Simpson 1952; Ramage 1962; Nieto et al. 2008). The last stage is marked by a ~~significant~~ considerable decrease in precipitation.

The life cycle of the SH COLs in terms of the geopotential height (Figure 5) is similar to that described by Nieto et al. (2008) for the NH COLs, except the pressure level shown in the schematic of Nieto et al. (2008) depicts the geopotential field at 200 hPa (see their Fig. 4) while the analyses in our study refers to 300 hPa which is the level that has been found where the maximum intensity of the SH COLs occur (see Fig. 3a-b). During the initial stages of the lifecycle, the composite geopotential height shows an elongated appearance with a westward tilt, while a more symmetric and barotropic structure occurs in the final stages. It is interesting to note that the absolute Z_{300} minimum associated with a cyclonic COL centre is found in the tear-off stage (~8850 gpm) which occurs 24h before the time of maximum cyclonic ξ_{300}. This means there are differences in the COL lifecycle with respect to vorticity and geopotential, and this has not been previously documented. Despite the difference between vorticity and geopotential, the stages outlined in the Nieto's conceptual model and confirmed in this study can be used as a guide for the different stages of the COL development regardless of the region in which the COL occurs.

The precipitation composite (Figure 5a) exhibits an asymmetry and a large variation in time where the peak values occur from mature to decay stages. This agrees with earlier findings that examined the precipitation associated with COLs in South America

(Satyamurty and Seluchi 2007; Godoy et al. 2011; Bozkurt et al. 2016), but contradicts the report of Delgado et al. (2007) who found the maximum precipitation in Mediterranean COLs during the earlier stages, suggesting there may be regional differences among COLs with respect to their properties and life cycle.

The evolution of the SH COLs shows that the cold core structure (Figure 5d) is largely modified throughout the life cycle, since the greatest extent occurs between the upper-level and cut-off stages, but it reduces horizontally and vertically in the decay stage (vertical fields are shown in the Supplementary Material). During the initial stages, the largest warming occurs in the rearward region (ridge) due to the upper-level convergence and descending air that are heated by adiabatic compression. However, warm anomalies extend eastward in the final stages which agrees well with previous studies in which cold cores are destroyed by diabatic heating (Hoskins et al. 1985; Sakamoto and Takahashi 2005; Garreaud and Fuenzalida 2007). Since the aspects described above are typical of the strongest COLs and assuming that numerical models are capable to capture these aspects, models could be used in practice to predict the COL evolution.

The study of the lifecycle of COLs continues by analysing the vertical tilt (Figure 6). Tilt is determined for different stages before and after the time of maximum intensity in ξ_{300}. The maximum vertical tilt is observed at the first step (60h before time zero) and at low levels (900-700 hPa) when the distance between the 900 and 300 hPa centres is slightly higher than 2^{o}. The westward vertical tilt observed during the early stages is typical of baroclinic systems, though this tilt is much less than that found in extratropical cyclones (Bengtsson et al. 2009). The vertical tilt reduces as the system approaches its maximum intensity, when the distances for vorticity centres between lower and upper levels do not exceed 1.0^{o}. Once COLs start decaying, their structure becomes quasi-barotropic and even exhibit a reverse tilt (i.e. an eastward vertical tilt), particularly at high levels. An important feature is the maximum tilt at lower levels observed particularly in the early and late stages. Similar results were found by Randel and Stanford (1985) for the life cycle of baroclinic waves at austral mid-latitudes.

6 Relationship of the precipitation to environmental features

6.1 Upper-level forcing and moisture content

This section analyses how environmental aspects affect precipitation such as the intensity of COLs and their moisture content. Figure 7 provides a quantitative analysis of the cumulative precipitation measured along each identified COL with respect to different intensity ranges, expressed in terms of statistical boxplots (or box and whisker diagram). This is obtained by accumulating all values between the first and last track points, computed over a 5^{o} spherical cap (about 500 km radius) centred on the ξ_{300} minimum. The precipitation is not the instantaneous value, it is the precipitation obtained from the forecast model accumulated over a 6-h period with 12 hour forecast lead time (which prevents the influence of model spinup). On the basis of this result, it is clear that the mean cumulative precipitation is affected by the COL intensity. The median does not change much with intensities less than -8 $\times$ 10^{-5} s^{-1}, but a ~~significant~~considerable increase is observed for the stronger COLs (intensities smaller than -8 $\times$ 10^{-5} s^{-1}) over those of smaller intensities (greater than -8 $\times$ 10^{-5} s^{-1}). The increase is particularly marked for the 75th percentile, meaning that high rainfall amounts are much more frequent in stronger COLs compared to weaker systems. Extreme outliers are omitted from the analysis due to their large values, which are expected when boxplots are applied to large datasets (Hofmann et al. 2017). Regardless of the definition of 'outside value', a close inspection of the largest cumulative precipitation events (> 100 mm per event) reveals that these occur for different intensity types, suggesting that other factors, besides upper-level COL intensity, may be important to trigger extreme precipitation, such as moisture and instability.

It is expected that the moisture available in the environment surrounding a COL is important to produce precipitation. To ~~check~~ test this hypothesis, we performed a similar experiment to that of Field and Wood (2007) where they categorized lower tropospheric cyclones into different groups according to their intensity (measured in terms of surface wind speed) and moisture (measured in terms of column-integrated water vapor). In the present study, composites of precipitation for the COLs are produced conditioned on ξ_{300} (increasing from left to right) and precipitable water (increasing from bottom to top) (Figure 8). Mean values of the nine composites were calculated for the ξ_{300} COLs relative to the time of maximum intensity averaged within 5^{o} spherical arc radius centred on the ξ_{300} minimum. As expected, the precipitation increases simultaneously with both intensity and moisture. The composite with the greatest intensities and moisture content has the largest area-average accumulated precipitation over the 5^{o} region (26.1 mm), which is the sum over the whole lifecycle of all selected storms in the composite. However, for this composite the standard deviation shows significant variation in precipitation among the COLs (see Figure S4 in the Supplementary Material). In contrast, the lowest area-average accumulated precipitation is observed for the composite with the smallest intensities and moisture content, which corresponds to 13.8 mm. The wetter composites seem to be associated with the most widespread precipitation, whereas the drier composites have precipitation occurring over reduced areas. These results suggest that moisture is an important factor controlling the precipitation area, though the intensity seems to influence the magnitude of precipitation in the COLs which may be linked to the strength of the low-level convergence. This hypothesis requires further inves~~r~~tigation.

It can be seen that the composite with most precipitation (top right of Figure 8) does not have the deepest geopotential centre, but instead the three driest composites have a deeper centre than the three composites with greatest moisture content. The reason for weaker intensities observed in the COLs with high precipitation may be explained by the modification of the dynamical structure of COLs due to diabatic latent heating which induces an upper-level anticyclonic PV anomaly, as discussed in many studies (Davies and Emanuel 1991; Reed et al. 1992; Stoelinga 1996; Ahmadi-Givi et al. 2004). Composites produced relative to the time of maximum precipitation indicate similar results, these are given in the Supplementary Material (Section 3).

6.2 Dependence on vertical structure

Some common characteristics that can be used to develop conceptual models of COLs have been identified in this study, though there seems to be a significant variation among the observed COLs suggesting the existence of different types of upper-level cyclonic vortices differing in terms of their vertical structure and weather-related impacts such as precipitation. Figure 9 summarises the differences in characteristics between two different types of COLs: the first one (Fig. 9b) represents the most intense COLs obtained from the composite of the 200 strongest COLs; the second type (Fig. 9a) represents the average COLs obtained from all identified COLs which corresponds to 11,542 COLs. This shows how the intensity of COLs affects their structure. For the time of maximum intensity, composites of the most intense COLs show a deep vertical structure with well-defined cyclones reaching into the lower troposphere. The vertical coupling induces strong upward vertical motion and enhanced low-level moisture convergence, contributing to a large amount of precipitation. It has been suggested that the coupling described above occurs when the low-level thermal advection has initiated

(Deveson et al. 2002) hinting to a possible synergistic interaction between upper and lower level features, though there may be different ways for classifying cyclones (Evans et al. 1994; Sinclair and Revell 2000; Catto 2016). The composites produced using all identified COLs representing the average COLs, show a much shallower structure with a well-defined vortex only at high levels. For this case, the perturbation gradually weakens with decreasing height and is replaced by an anti-cyclonic circulation on the western side at the surface. Reduced precipitation rates are observed for this type of COL because of the weakened vertical motions and decoupling between upper and lower level disturbances.

A track matching algorithm was applied to the categories described above in order to determine the vertical depth of the COLs. This is done by searching for corresponding vorticity minima at pressure levels lower than 300 hPa, starting by matching the 400-hPa vorticity tracks and successively for other levels down to the 1000-hPa level or the lowest pressure level where the match is found, using the same criteria and thresholds. This is done by applying a prescribed value for the mean separation distance between tracks (chosen here to be 5 degrees geodesic) which overlaps in time for at least one per cent of the track points. We found that only 19.4% of the average COLs have a corresponding surface cyclone, but the percentage rises to 65% when the COLs are the strongest systems. This confirms earlier findings that only a few COLs reach the surface and indicates a possible relation between intensity of COLs and their vertical depth.

7 Discussion and conclusions

This paper provides the first robust view of the structure, lifecycle and properties of SH COLs including how their precipitation depends on their structure. The present study has concentrated on the analysis of the 200 most intense COLs (> 98th percentile) located in the SH. This provides a better understanding of the behaviour of COLs and a useful forecasting aid. Although there is no single concept of the structure and evolution of COLs because of their diverse nature, some common characteristics can be identified by the use of a compositing method that allows the identification of key features of the most intense COLs. Some of the well-known features of conceptual models reported in previous studies are found here and presented herein including: the horizontal and vertical circulation structures, the cold and warm cores and their associated baroclinic zones, the STE caused by tropopause folding, and the precipitation characteristics and other related features.

The results reported in this study support earlier case studies of COLs that have found a roughly symmetrical circulation at upper levels with maximum winds at about 300 hPa, creating a region of strong horizontal and vertical wind shear. The contrast between the cold air in the vortex centre and the relatively warm air at the periphery produces a distinctly frontal structure on the borders of these systems. The sharpest temperature gradients in COLs are found across the edges of the mid-upper tropospheric cold core where the baroclinic zones normally propagate downstream, which agrees well with the conceptual model described by Keyser and Shapiro (1986) for upper-level fronts. The STE is a consequence of the tropopause deformation in COLs where large amounts of stratospheric air are transported into the troposphere. Our results are consistent with earlier reports indicating that the vertical distribution of PV and ozone are significantly modified in strong COLs. In the mature stage, the vortex tropopause is lowered to around 400-500 hPa, although deeper stratospheric intrusion events can sink the tropopause down to 600-700 hPa, as reported in Hoskins et al. (1985) and observed by individual cases in the present study (see the Supplementary Material, Section 5).

A key finding of this study, which has not been addressed in previous studies, is that there are clearly distinct differences in the vertical structure of the SH COLs which can be demonstrated by means of two different types of COLs. The two models of COLs are similar in terms of their spatial distribution of vertical motions and precipitation but they differ with respect to their magnitude. The major difference between the two groups lies in the contrast between a deep COL structure extending down to the surface and a COL confined at mid-upper levels, suggesting that the differences observed in the vertical depth of the COLs are in part a consequence of the precipitation amount. In this sense, inspection of synoptic weather charts and satellite images provide additional evidence that not all COLs have the same structure and precipitation characteristics and that regional perspectives depending on local topography and surface condition features are important.

We have for practical reasons restricted the analysis to the COLs that affect subtropical regions. However, similarities and differences between COLs and other tropopause vortex types (including tropical and polar vortices) are not clearly defined. Some of the structural properties of COLs that have been identified in this study can be found as dominant features in TPVs (Cavallo and Hakim 2010), such as the vertical motions where air rises (sinks) east (west) of the vortex centre, and the cold and warm anomalies in the troposphere and stratosphere, respectively. These systems can be linked to RWB events as both are isolated PV anomalies but COLs are located equatorward of the jet stream while TPVs poleward of the jet.

In comparison to TTVs, the COLs studied here have properties comparable to those described in previous studies such as a lowered tropopause and a warm anomaly superimposed on a cold anomaly (Frank 1970; Kousky and Gan 1981; Mishra et al. 2001). However, the vertical motion in TTVs exhibits a more symmetrical pattern, with sinking air near the vortex centre and rising air at the periphery (Kousky and Gan 1981). Moreover, while Kousky and Gan (1981) observed that the deepest convective clouds are seen in the direction of the movement which is often westward in tropical latitudes, our results indicate that the largest precipitation occurs in the eastern side of the COLs. Nevertheless, it might be interesting in future studies to contrast the vertical structure and precipitation of all tropopause vortices, for example, using as identification field the potential temperature on the 2.0 PVU surface.

It is also useful to point out how the characteristics of the SH COLs studied here (e.g. precipitation) compare with those associated with NH COLs such as the systems observed in the Iberian Peninsula and Mediterranean regions (Nieto et al. 2005; 2008; Delgado et al. 2007; Porcù et al. 2007). The distribution of precipitation and cloud cover (the last one not shown here) reproduces the main rainfall band located in the leading edge of the COL (east flank) but does not demonstrate the secondary region in the rear edge of the system (west flank), which in turn is associated with a descending branch. We found that the peak precipitation occurs from the mature to decay stages, which is in agreement with earlier studies on COLs that occurred in South America (Satyamurty and Seluchi 2007; Godoy et al. 2011; Bozkurt et al. 2016). However, most of the precipitation is found in earlier stages in NH COLs (Delgado et al. 2007; Nieto et al. 2008), and this may be due to regional differences or the way in which a COL is defined. Differences are also seen by comparing COLs with extratropical cyclones (Bengtsson et al. 2009) which produce more precipitation in their intensifying phase. One possible explanation might be that deep COLs and surface cyclones are often part of the same phenomenon in the development of an upper-level precursor prior to the low-level cyclone, as discussed by Mikyfunatsu et al. (2004).

Although COLs are often referred to as cold pools due to their well-defined cold-core structure, a general consensus on the location of the cold anomalies is still missing. One particularly important factor in determining the vertical location of the cold core of

COLs may be the dynamical tropopause position which varies depending on factors such as latitude, season and synoptic situation. Our results show that the tropopause intersects in the COL centre inside the cold core (just above the coldest anomalies) within a region of sharp temperature gradient, also called frontal or baroclinic zone. However, there have been many studies on COLs using methods based on criteria that search for cold cores at very high levels (for example, between 200 and 300 hPa) in both the southern and northern hemispheres (Nieto et al. 2005; Gimeno et al. 2007; Porcù et al. 2007; Reboita et al. 2010; Muñoz et al. 2019) which may result in differences between studies, as recently discussed by Pinheiro et al. (2019). Unfortunately the lack of studies focusing on the structure of COLs and the difference between hemispheres does not allow us to determine whether the difference in interpretation is a result of the regional peculiarities. There is thus a clear need for more observational studies on COLs in both hemispheres to create a better conceptual framework encompassing the variety of the structures presented in COLs and other cold core vortex types.

To summarize our current understanding of COLs, a schematic depiction of the structural features is presented in Fig. 10. This schematic is adapted from Llasat et al. (2007), which is based on the typical properties of Mediterranean COLs, and despite the subjective interpretation there is agreement on the vertical profile of COLs since both schematics denote similar features. The most notable difference is the pressure level of the warm anomalies which is considerably lower (~300 hPa) in Llasat et al. (2007) compared to those of our composite COL. sThe schematic presented in Fig. 10 illustrates the dominant mechanisms and key properties of COLs such as their circulation structures, tropopause folding, cold and warm cores and their associated baroclinic zones. This schematic together with results shown in this study may serve as a reference guide for the diagnosis of the structural and precipitation features in COLs, helping meteorologists understand weather patterns and produce better forecasts.

Although we have not specifically addressed the issue of forecasting ability of numerical weather prediction (NWP) models, this is a problem of great scientific importance for understanding problems typically found in predicting COLs. Many studies have demonstrated that diabatic effects play an important role in the development of different vortex types, with radiative cooling and latent heating contributing to strengthening and weakening, respectively (Hoskins et al. 1985; Katzfey and Mcinnes 1996; Sakamoto and Takahashi 2005; Garreaud and Fuenzalida 2007; Cavallo and Hakim 2010). It is therefore fundamental to explore the predictive skill of forecast systems for COL activity, as has been done for extra-tropical and tropical cyclones (Froude et al. 2007; Hodges and Klingaman 2019). Moreover, better predictions require a detailed understanding of the processes that govern the development of COLs, which is beyond the scope of this paper, but will be explored in future research.

This work could also be extended to investigate the cloud properties, but the reanalyses are not well constrained in terms of clouds since the cloud cover is not assimilated into the reanalyses, but instead is predicted by a short range forecast using the same atmospheric model used by the ERAI reanalysis. The use of remote sensing data, such as the International Satellite Cloud Climatology Project data set (ISCCP), could be used to more precisely capture the cloud structure of COLs, as has been performed more generally for extratropical cyclones (Field and Wood 2007; Hawcroft et al. 2012; 2017).

Finally, despite the contribution of this study to our understanding of COLs, it is unclear whether the results showed herein would be robust enough to represent the structure and evolution of all COLs around the world given the different vortex types. The problem concerning the variety of methods used to identify COLs (Pinheiro et al. 2019) raises the question of whether the different criteria are due to the different conceptual models as a result of the interpretation or differences in structure between the COLs in the Northern and Southern Hemispheres. For this reason we believe that further studies are needed to investigate a possible regional dependence of the COL structure and its evolution as COLs may exhibit different characteristics when they occur in different regions, so that it would be possible to better understand how COLs behave in certain regions while also allowing us to adjust the identification methods to particular geographical locations. Another problem of great scientific importance is how large-scale atmospheric modes of variability influence on COL related properties (such as location, intensity and precipitation). This is crucial for understanding the climate and its variation, and more specifically the effect of the large-scale modes of variability on the seasonal and sub-seasonal prediction of COLs.

Acknowledgements

We thank the anonymous reviewers for their constructive comments which have helped to improve the paper. The work was partly sponsored by CNPq (Conselho Nacional de Desenvolvimento Científico e Tecnológico) and CAPES (Coordenação de Aperfeiçoamento de Pessoal de Nível Superior). The University of Reading (England) and National Institute for Space Research (INPE, Brazil) provide support through computing resources. The authors are also grateful to Jorge Conforte for his help in producing a plot.

References

Ahmadi-Givi, F., Graig, G.C, Plant, R.S. (2004) The dynamics of a midlatitude cyclone with very strong latent-heat release. *Quarterly Journal of the Royal Meteorological Society* **130**(596), 295-323.

Bell, G.D. and Bosart, L.F. (1993) A case study diagnosis of the formation of an upper-level cutoff cyclonic circulation over the eastern United States. *Monthly Weather Review* **121**(6), 1635-1655.

Bengtsson, L., Hodges, K., Keenlyside, N. (2009) Will extratopical storms intensify in a warmer climate? *Journal of Climate* **22**(9), 2276-2301.

Bozkurt, D., Rondanelli, L., Garreaud, R. and Arriagada, A. (2016) Impact of warmer eastern tropical Pacific SST on the March 2015 Atacama floods. *Monthly Weather Review* **144**(11), 4441-4460.

Campetella, C.M. and Possia, N.E. (2007) Upper-level cut-off lows in southern South America. *Meteorology and Atmospheric Physics* **96**(1-2), 181-191.

Catto, J.L, Shaffrey, L.C. and Hodges, K.I. (2010) Can climate models capture the structure of extratropical cyclones? *Journal of Climate* **23**(7), 1621-1635.

Catto, J.L. (2016) Extratropical cyclone classification and its use. *Reviews of Geosphysics* **54**(2), 486-520.

Cavallo, S.M. and Hakim, G.J. (2010) Composite structure of tropopause polar cyclones. *Monthly weather review* **138**(10), 3840-3857.

Clarke, L.C. and Renard, R.J. (1966) The U.S. Navy numerical frontal analysis scheme: further development and a limited evaluation. *Journal of Applied Meteorology* **5**(6), 764-777.

Dacre, H.F., Hawcroft, M.K., Stringer, M.A. and Hodges, K.I. (2012) An extratropical cyclone atlas: a tool for illustrating cyclone structure and evolution characteristics. *Bulletin of the American Meteorological Society* **93**(10), 1497-1502.

Davis, C.A. and Emanuel, K.A. (1991) Potential vorticity diagnostics of cyclogenesis. *Monthly Weather Review* **119**(8), 1929-1953.

Dee, D.P., Uppala, S.M. and Simmons, A.J., Berrisford, P. Poli P et al (2011) The ERAI reanalysis: configuration and performance of the data assimilation system. *Quarterly Journal of the Royal Meteorological Society* **137**(656), 553-597.

Delgado, G., Redaño, G., Lorente, J., Nieto, R., Gimeno, L., Ribera, P., Barriopedro, D., García-Herreras, R. and Serrano, A. (2007) Cloud cover analysis associated to cut-off low pressure systems over Europe using Meteosat imagery. *Meteorology and Atmospheric Physics* **96**(1-2), 141-157.

Deveson, A.C.L., Browning, K.A. and Hewson, T.D. (2002) A classification of FASTEX cyclones using a height-attributable quasi-geostrophic vertical-motion diagnostic. *Quarterly Journal of the Royal Meteorological Society* **128**(579), 93-117.

Evans, M.S., Keyser, D., Bosart, L.F. and Lackman, G.M. (1994) A satellite-derived classification scheme for rapid maritime cyclogenesis. *Monthly Weather Review* **122**(7), 1381-1416.

Favre, A., Hewitson, B., Tadross, M., Lennard, C. and Cerezo-Mota, R. (2012) Relationships between cut-off lows and the semiannual and southern oscillations. *Climate Dynamics* **38**(7-8), 1473-1487.

Field, P.R. and Wood, R. (2007) Precipitation and cloud structure in midlatitude cyclones. *Journal of Climate* **20**(2), 233-254.

Frank, N.L. (1970) On the energetics of cold lows. In: Symposium on Tropical Meteorology. Proceedings… *American Meteorological Society* EIV1-EIV6.

Froude, L.S., Bengtsson, L., and Hodges, K.I. (2007) The prediction of extratropical storm tracks by the ECMWF and NCEP ensemble prediction systems. *Monthly weather review*, **135**(7), 2545-2567.

Fuenzalida, H.A., Sánchez, R. and Garreaud, R.D. (2005) A climatology of cutoff lows in the Southern Hemisphere. *Journal of Geophysical Research* 110:D18101.

Gan, M.C. and Rao, V.B. (1996) Case studies over South America. *Meteorological Applications* **3**, 359-367.

Gan, M.A. and dal Piva, E. (2013) Energetics of a Southeastern Pacific cut-off low. *Atmospheric Science Letters* **14**(4), 272-280.

Garreaud, R.D. and Fuenzalida, H.A. (2007) The influence of the Andes on cutoff lows: a modeling study. *Monthly Weather Review* **135**(4), 1596-1613.

Gimeno, L., Nieto, R. and Trigo, R.M. (2007) Decay of the Northern Hemisphere stratospheric polar vortex and the occurrence of cut-off low systems: An exploratory study. *Meteorology and Atmospheric Physics* **96**(1-2), 21-28.

Godoy, A.A., Possia, N.E., Campetella, C.M. and Skabar, Y.G. (2011) A cut-off low in southern South America: dynamic and thermodynamic processes. *Revista Brasileira de Meteorologia* **26**(4), 503-514.

Griffiths, M., Reeder, M.J., Low, D.J. and Vincent, R.A. (1998) Observation of a cut-off Low over southern Australia. *Quarterly Journal of the Royal Meteorological Society,* **124**(548), 1109-1132.

Hawcroft, M.K., and Shaffrey, L.C., Hodges, K.I. and Dacre, H.F. (2012) How much Northern Hemisphere precipitation is associated with extratropical cyclones? *Geophysical Research Letters* **39**(24), 1-7.

Hawcroft, M.K., Shaffrey, L.C., Hodges, K.I. and Dacre, H.F. (2016) Can climate models represent the precipitation associated with extratropical cyclones? *Climate Dynamics* **47**(3-4), 679-695.

Hawcroft, M., Dacre, H., Forbes, R., Hodges, K., Shaffrey, L. and Stein, T. (2017) Using satellite and reanalysis data to evaluate the representation of latent heating in extratropical cyclones in a climate model. *Climate Dynamics* **48**(7-8), 2255-2278.

Hodges, K.I. (1995) Feature tracking on the unit sphere. *Monthly Weather Review* **123**(12), 3458-3465.

Hodges, K.I. (1996) Spherical nonparametric estimators applied to the UGAMP model integration for AMIP. *Monthly Weather Review* **124**(12), 2914-2932.

Hodges, K.I., and Klingaman, N.P. (2019) Prediction errors of tropical cyclones in the western North Pacific in the Met Office global forecast model. *Weather and Forecasting*, **34**(5), 1189-1209.

Hofmann, H., Wickham, H. and Kafadar, K. (2017) Value plots: Boxplots for large data. *Journal of Computational and Graphical Statistics* **26**(3), 469-477.

Hoskins, B.J. (1971) Atmospheric frontogenesis models: some solutions. *Quarterly Journal of the Royal Meteorological Society* **97**(412), 139-153.

Hoskins, B.J., Mcintyre, M.E. and Robertson, A.W. (1985) On the use and significance of isentropic potential vorticity maps. *Quarterly Journal of the Royal Meteorological Society* **111**(470), 877-946.

Hsieh, Y. (1949) An investigation of a selected cold vortex over North America. *Journal of Meteorology* **6**(6), 401-410.

Katzfey, J.J., and Mcinnes, K.L. (1996) GCM simulations of eastern Australian cutoff lows. *Journal of climate*, **9**(10), 2337-2355.

Kelley, W.E. and Mock, D.R. (1982) A diagnostic study of upper tropospheric cold lows over the western North Pacific. *Monthly Weather Review* **110**(6), 471-480.

Kentarchos, A.S., Roelofs, G.J. and Lelieveld, J. (1999) Model study of a stratospheric intrusion event at lower midlatitudes associated with the development of a cutoff low. *Journal of Geophysical Research Atmospheres* **104**(D1), 1717-1727.

Keyser, D. and Shapiro, M.A. (1986) A review of the structure and dynamics of upper-level frontal zones. *Monthly Weather Review* **114**(2), 452-499.

Knippertz, P. and Martin, J.E. (2005) Tropical plumes and extreme precipitation in subtropical and tropical West Africa. *Quarterly Journal of the Royal Meteorological Society* **131**(610), 2337-2365.

Knowland, K.E., Doherty, R.M. and Hodges, K.I. (2015) The effects of springtime mid-latitude storms on trace gas composition determined from the MACC reanalysis. *Atmospheric Chemistry and Physics* **15**(6), 3605-3628.

Kousky, V.E. and Gan, M.A. (1981) Upper tropospheric cyclonic vortices in the subtropical South Atlantic. *Tellus* **33**(6), 538-551.

Kuo, H.L. (1949) Dynamic instability of two-dimensional non-divergent flow in a baroclinic atmosphere. *Journal of Meteorology* **6**(2), 105-122.

Llasat, M.C., Martín, F., Barrera, A. (2007) From the concept of “Kaltlufttropfen” (cold air pool) to the cut-off low. The case of September 1971 in Spain as an example of their role in heavy rainfalls. Meteorology and Atmospheric physics 96(1-2), 43-60.

Marques, R.F.C. and Rao, V.B. (2000) Interannual variations of blockings in the Southern Hemisphere. *Journal of Computational Physics* **105**(D4), 4625-4636.

Mikyfunatsu, B., Gan, M.A. and Caetano, E. (2004) A case study of orographic cyclogenesis over South America. *Revista Atmosfera* **17**(2), 91-113.

Mishra, S.K., Rao, V.B. and Gan, M.A. (2001) Structure and evolution of the large-scale flow and an embedded upper-tropospheric cyclonic vortex over Northeast Brazil. Monthly weather review 129(7), 1673-1688.

Muller, A., Reason, C.J.C. and Fauchereau, N. (2008) Extreme rainfall in the Namib Desert during late summer 2006 and influences of regional ocean variability. *International Journal of Climatology: A Journal of the Royal Meteorological Society* **28**(8), 1061-1070.

Muñoz, C., Schultz, D. and Vaughan, G. (2019) A midlatitude climatology and interannual variability of 200-and 500-hPa cut-off lows. *Journal of Climate* **33**(6), 2201-2222.

Muofhe, T.P., Chikoore, H., Bopape, M.J., Nethengwe, N. S., Ndarana, T. and Gift, T.R. (2020) Forecasting Intense Cut-Off Lows in South Africa Using the 4.4 Km Unified Model. *Preprints.*

Ndarana, T. and Waugh, D.W. (2010) The link between cut-off lows and Rossby wave breaking in the Southern Hemisphere. *Quarterly Journal of the Royal Meteorological Society* **136**(649), 869-885.

Ndarana, T., Rammopo, T.S., Chikoore, H., Barnes, M.A., and Bopape, M.J. (2020) A quasi-geostrophic diagnosis of the zonal flow associated with cut-off lows over South Africa and surrounding oceans. *Climate Dynamics, Preprints.*

Nieto, R., Gimeno, L., de la Torre, L., Ribeira, P., Gallego, D., García-Herrera, R. et al (2005) Climatological features of cutoff low systems in the Northern Hemisphere. *Journal of Climate* **18**(16), 3085-3103.

Nieto, R., Sprenger, M., Wernli, H., Trigo, R.M. and Gimeno, L. (2008) Identification and climatology of cut-off low near the tropopause. *Annals of the New York Academy of Sciences* **1146**(1), 256-290.

Palmén, E. (1949) Origin and structure of high-level cyclones south of the maximum westerlies. *Tellus* **1**(1), 22-31.

Palmén, E. and Newton, C.W. (1969) *Atmospheric circulation systems: their structure and physical interpretation.* New York: Academic Press.

Pinheiro, H.R., Hodges, K.I., Gan, M.A. and Ferreira, N.J. (2017) A new perspective of the climatological features of upper-level cut-off lows in the Southern Hemisphere. *Climate Dynamics* **48**(1-2), 541-559.

Pinheiro, H.R., Hodges, K.I. and Gan, M.A. (2019) Sensitivity of identifying Cut-off Lows in the Southern Hemisphere using multiple criteria: implications for numbers, seasonality and intensity. *Climate Dynamics* **53**(11), 6699-6713.

Pinheiro, H.R., Hodges, K.I. and Gan, M.A. (2020) An intercomparison of Cut-off Lows in the subtropical Southern Hemisphere using recent reanalyses: ERA-Interim, NCEP-CFSR, MERRA-2, JRA-55, and JRA-25. *Climate Dynamics* **54**, 777-792.

Pook, M.J., Mcintosh, P.C. and Meyers, G.A. (2006) The synoptic decomposition of cool-season rainfall in the southeastern Australian cropping region. *Journal of Applied Meteorology and Climatology* **45**(8), 1156-1170.

Porcù, F., Carrassi, A., Medaglia, C.M., Prodi, F. and Mugnai, A. (2007) A study on cut-off low vertical structure and precipitation in the Mediterranean region. *Meteorology and Atmospheric Physics* **96**(1-2), 121-140.

Price, J.D. and Vaughan, G. (1992) Statistical studies of cut-off low systems. *Annales Geophysicae* **10**, 96-102.

Price, J.D. and Vaughan, G. (1993) The potential for stratosphere-troposphere exchange in cut-off low systems. *Quarterly Journal of the Royal Meteorological Society* **119**(510), 343-365.

Qi, L., Leslie, L.M., and Zhao, S.X. (1999) Cut-off low pressure systems over southern Australia: climatology and case study. *International Journal of Climatology: A Journal of the Royal Meteorological Society*, **19**(15), 1633-1649.

Quispe, N. and Avalos, G. (2006) Intense snowstorm in the southern mountains of Peru associated to the incursion to the incursion of cut-off low-pressure systems at upper level. *In: International Conference on Southern Hemisphere Meteorology and Oceanography (ICSHMO)*, Foz do Iguaçu-Brazil, 1945-1958.

Ramage, C.S. (1962) The subtropical cyclone. *Journal of Geophysical Research* **67**(4), 1401-1411.

Randel, W.J. and Stanford, J.L. (1985) The observed life cycle of a baroclinic instability. *Journal of the Atmospheric Sciences* **42**(13), 1364-1373.

Reboita, M.S., Nieto, R., Gimeno, L., Rocha, R.P., Ambrizzi, T., Garreaud, R. and Kruger, L.F. (2010) Climatological features of cutoff low systems in the Southern Hemisphere. *Journal of Geophysical Research: Atmospheres* **115**, D17104.

Reboita, M.S. and Veiga, J.A.P. (2017) Synoptic and energetic analysis of a Cut-off Low that caused precipitation over the Atacama Desert in March, 2015 (Análise sinótica e energética de um VCAN que causou chuva no deserto do atacama em março de 2015) *Revista Brasileira de Meteorologia* **32**(1), 123-139.

Reed, R.J., Stoelinga, M.T. and Kuo, Y.H. (1992) A model-aided study of the origin and evolution of the anomalously high potential vorticity in the inner region of a rapidly deepening marine cyclone. *Monthly Weather Review* **120**(6), 893-913.

Reyers, M. and Shao, Y. (2019) Cutoff lows off the coast of the Atacama Desert under present day conditions and in the Last Glacial Maximum. *Global and Planetary Change* 102983.

Risbey, J.S., Pook, M.J., Mcintosh, P.C., Ummenhofer, C.C. and Meyers, G. (2009) Characteristics and variability of synoptic features associated with cool season rainfall in southeastern Australia. *International Journal of Climatology* **29**(11), 1595-1613.

Rondanelli, R., Gallardo, L. and Garreaud, R.D. (2002) Rapid changes in ozone mixing ratios at Cerro Tololo (30°10°S, 70°48°W, 2200 m) in connection with cut-off lows and deep troughs. *Journal of Geophysical* **107**, D23.

Sabo, P. (1992) Application of the thermal front parameter to baroclinic zones around cut-off lows. *Meteorology and Atmospheric Physics* **47**(2-4), 107-115.

Sakamoto, K., and Takahashi, M. (2005) Cut off and weakening processes of an upper cold low. *Journal of the Meteorological Society of Japan. Ser. II*, **83**(5), 817-834.

Satyamurty, P. and Seluchi, M.E. (2007) Characteristics and structure of an upper air cold vortex in the subtropics of South America. *Meteorology and Atmospheric Physics* **96**(3-4), 203-220.

Scherhag, R. (1939) Der kälteeinbruch mitte Dezember 1938. *Annalen Der Hydrographie und Maritimen Meteorologie* **67**, 142.

Shapiro, M.A. (1970) On the applicability of the geostrophic approximation to upper-level frontal-scale motions. *Journal of the Atmospheric Sciences* **27**(3), 408-420.

Silva Dias, P.L., Schubert, W.H. and Demaria, M. (1983) Large-scale response of the tropical atmosphere to transient convection. *Journal of the Atmospheric Sciences* **40**(11), 2689-2707.

Simpson, R.H. (1952) Evolution of the Kona Storm, a subtropical cyclone. *Journal of Meteorology* **9**(1), 24-35.

Sinclair, M.R. and Revell, M.J. (2000) Classification and composite diagnosis of extratropical cyclogenesis events in the Southwest Pacific. *Monthly Weather Review* **128**(4),1089-1105.

Singleton, A.T. and Reason, C.J.C. (2006) A Numerical model study of an intense cutoff low pressure system over South Africa. *Monthly Weather Review* **135**(3), 1128-1150.

Stoelinga, M.T. (1996) A potential vorticity-based study of the role of diabatic heating and friction in a numerically simulated baroclinic cyclone. *Monthly Weather Review* **124**(5), 849-874.

Trenberth, K.E. and Mo, K.C. (1985) Blocking in the Southern Hemisphere. *Monthly Weather Review* **113**(1), 3-21.

Wernli, H and Sprenger, M. (2007) Identification and ERA-15 climatology of potential vorticity streamers and cutoffs near the extratropical tropopause. *Journal of the Atmospheric Sciences* **64**(5), 1569-1586.

Figure/Captions

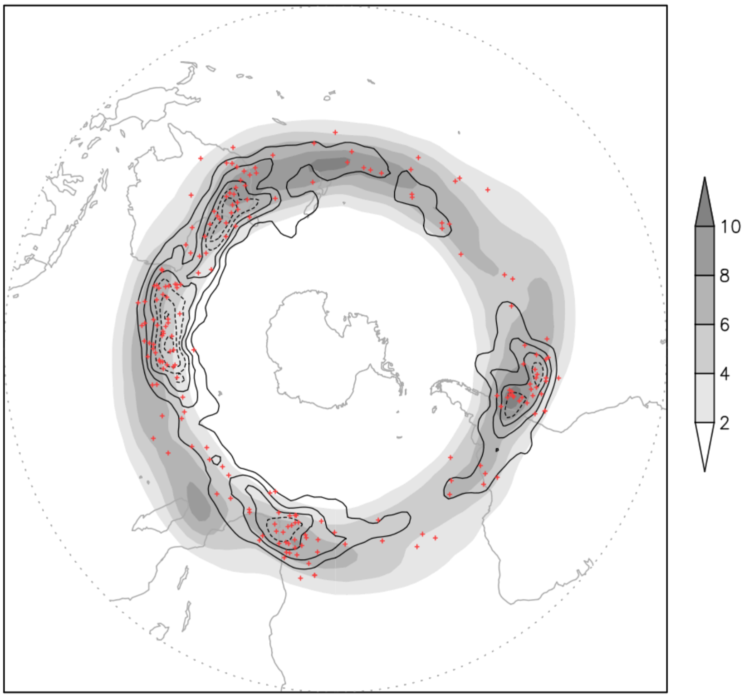

Figure 1 Seasonal track density of the Southern Hemisphere Cut-off Lows obtained from the 200 strongest (black lines) and average (shaded) Cut-off Lows. The contour interval is 0.1 unit for density ≤ 0.3 (solid line) and ≥ 0.4 (dotted line). Symbol plus (red colour) denotes the locations of the maximum intensity (with respect to the ξ_{300}) in

each track for the strongest COLs. Analysis is performed using the Cut-off Lows that match between the ξ_{300} and Z'_{300} from ERAI reanalysis for a 36-yr period (1979-2014). Unit is number per season per unit area, the unit area is equivalent to a 5° spherical cap ($\cong 10^6$ km^2).

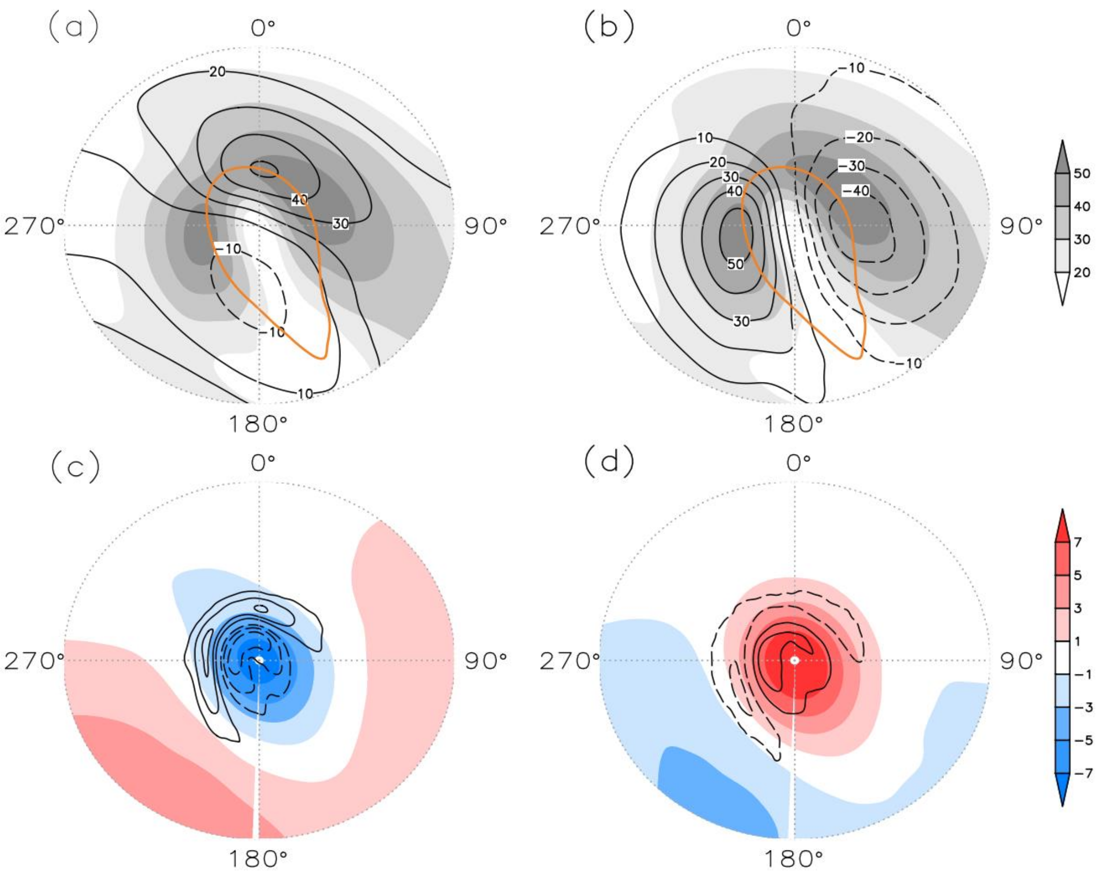

Figure 2 Horizontal composites for the 200 most intense Cut-off Lows that match between the ξ_{300} and Z'_{300} centred on the time and space relative to the ξ_{300} minimum. Fields are: a) zonal wind and b) meridional wind (black line) combined with wind speed (shaded) in m/s, and PV for the 2 PVU (orange line), all fields referred to 300 hPa; (c) and (d) are composites of temperature anomaly (shaded) in K and thermal frontal

parameter for contour intervals 0.4 × 10^{-10} K/(100 km)^2 at (c) 400 hPa and (d) 200 hPa. The distance from the centre of the COL composite to the edge is 15 degrees.

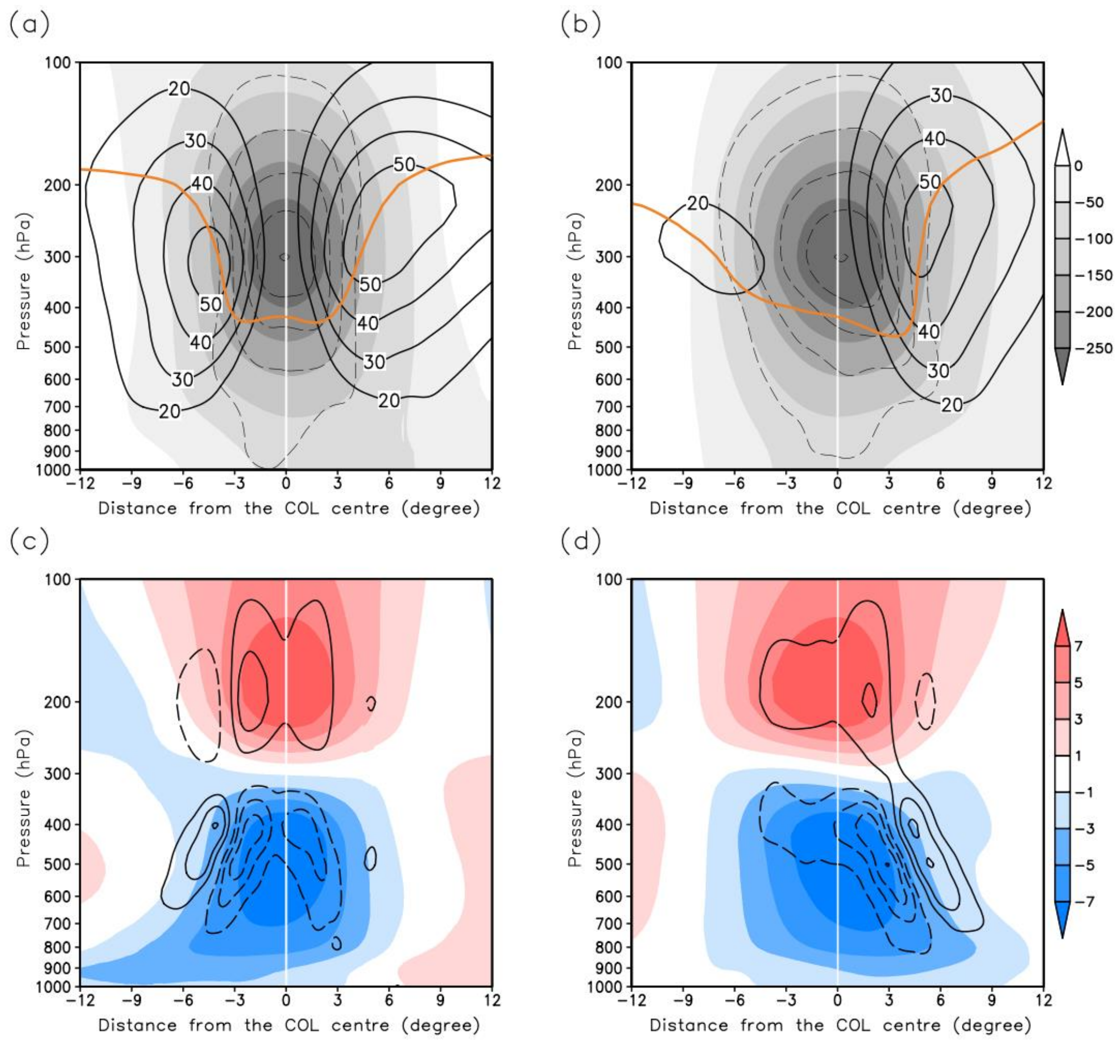

Figure 3 Composite vertical cross-sections along the (a),(c) west-east and (b),(d) south-north lines of the 200 most intense Cut-off Lows that match between the ξ_{300} and Z'_{300} centred on the time and space relative to the ξ_{300} minimum. Fields are (a),(b) wind speed (solid line) in m/s, geopotential height anomaly (shaded) for contour intervals 50 gpm, relative vorticity (dashed lines) in 10^{-5} s^{-1} for contour intervals 3.0 × 10^{-5} s^{-1}; and PV for the 2 PVU (orange line); (c) (d) temperature anomaly (shaded) in K; and thermal

frontal parameter (black lines) in for contour intervals 0.4×10^{-10} K/(100 km)^2, where solid (dashed) contours indicate positive (negative) values.

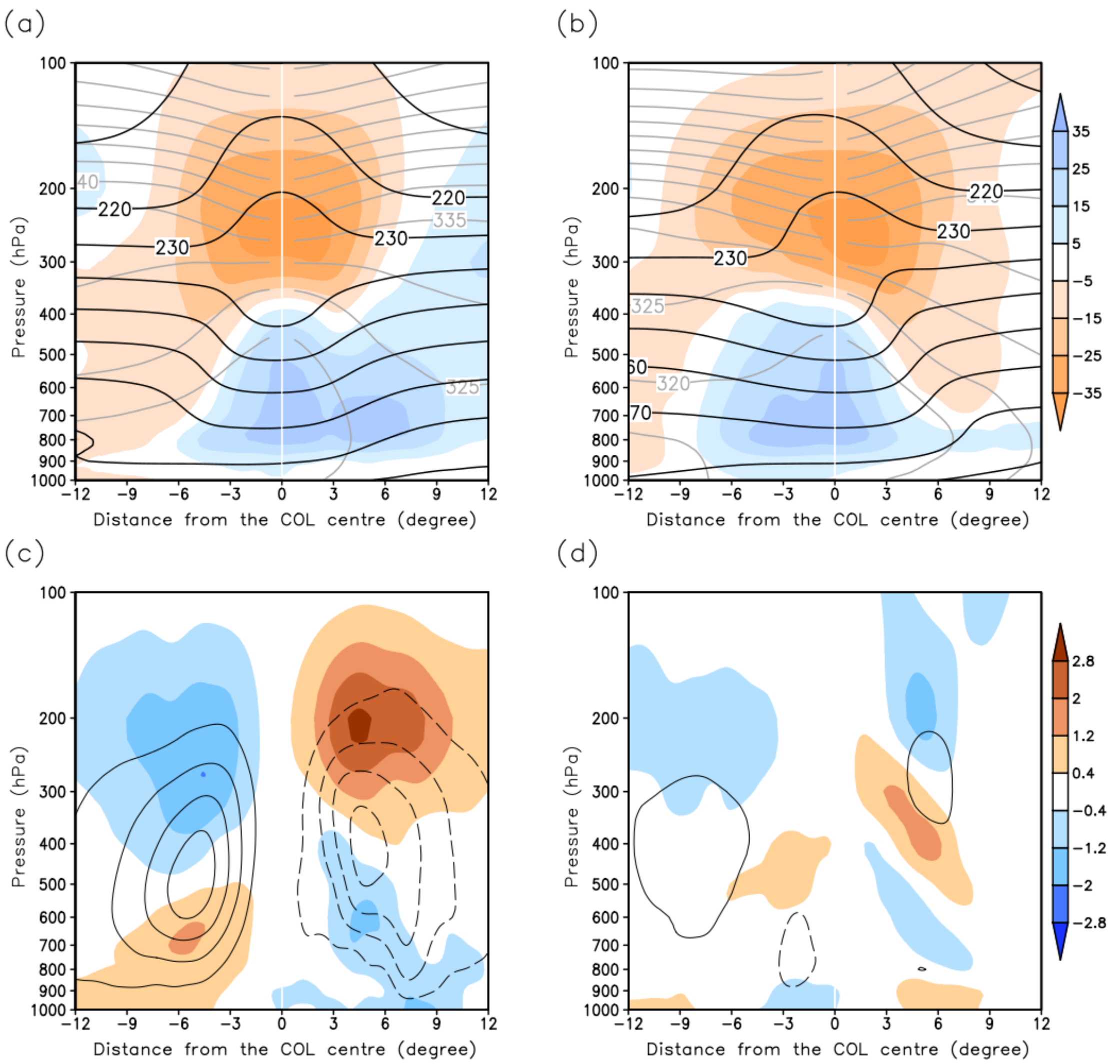

Figure 4 Composite vertical cross-sections along the (a),(c) west-east and (b),(d) south-north lines of the 200 most intense Cut-off Lows that match between the ξ_{300} and Z'_{300} centred on the time and space relative to the ξ_{300} minimum. Fields are (a),(b) relative humidity anomaly (shaded) in percentage, air temperature (black line) for contour intervals 10 K, potential temperature (grey line) for contour intervals 5 K, and (c),(d)

divergence (shaded) for contour intervals 0.8 10^{-5} s^{-1} and vertical velocity (black line) in contour intervals 0.1 Pa s^{-1}, where solid (dashed) contours indicate positive (negative) values.

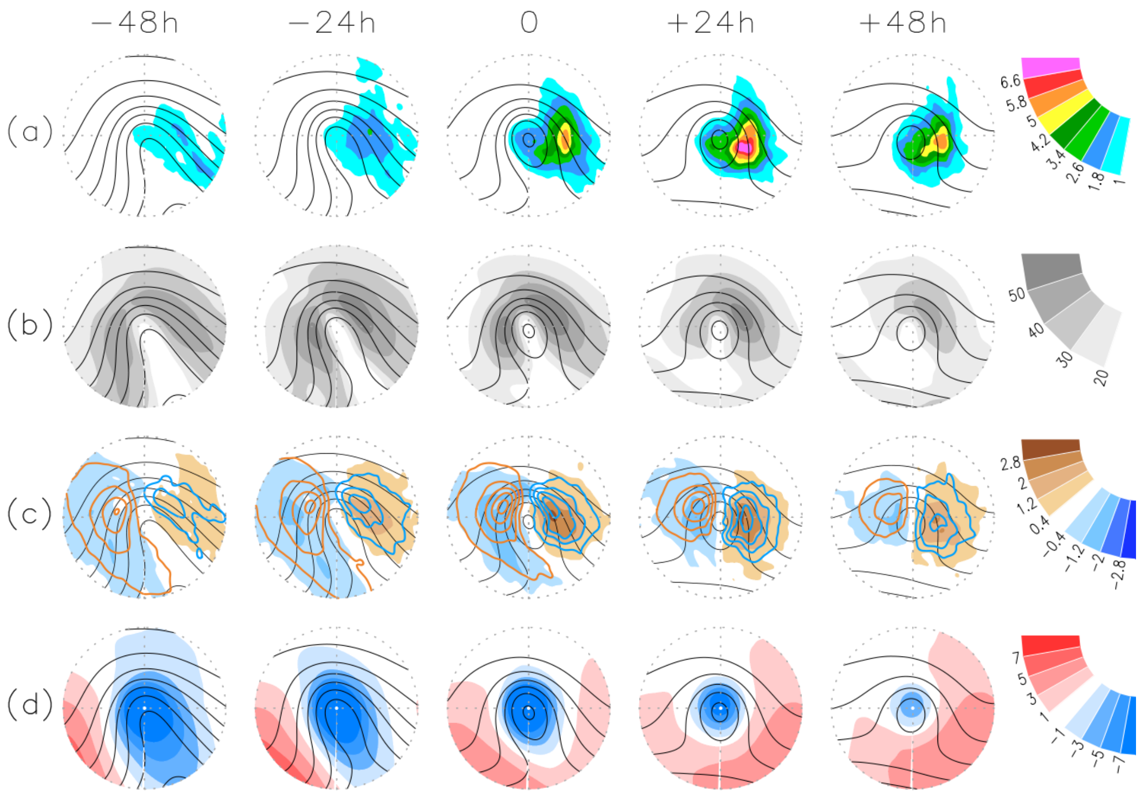

Figure 5 Life cycle composite of the Southern Hemisphere Cut-off Lows for the period between two days before and two days after the time of maximum intensity in ξ_{300} (day zero). Fields are: (a) 6-hourly accumulated precipitation in mm (shaded); (b) absolute wind speed in m/s (shaded); (c) divergence in 10^{-5} s^{-1} (shaded) and vertical velocity for contour intervals 0.1 Pa s^{-1} for positive (negative) values in orange (blue) colour; and (d) temperature anomaly in K (shaded). All fields are combined with the Z_{300} height for contour intervals 100 gpm (black contour).

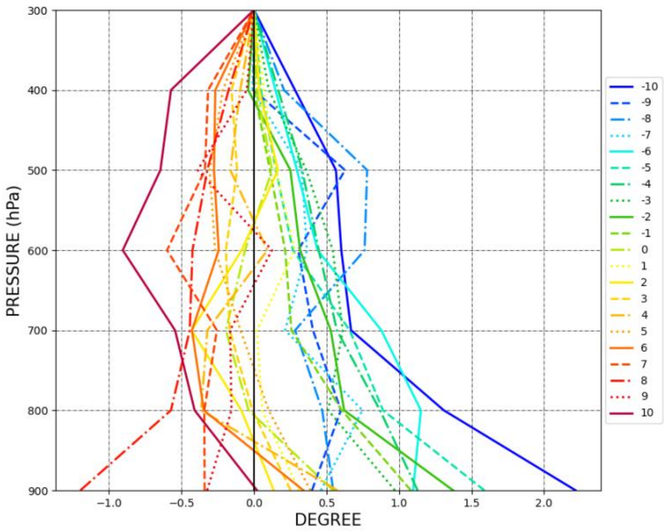

Figure 6 Vertical tilt life cycle composite for the Southern Hemisphere Cut-off Lows. Composite is obtained using the ξ_{300} Cut-off Lows. The time steps are for 6-hour interval, shown up to 60h on either side of the ξ_{300} minimum (time zero). Tilts are in geodesic angle from the ξ_{300} minimum.

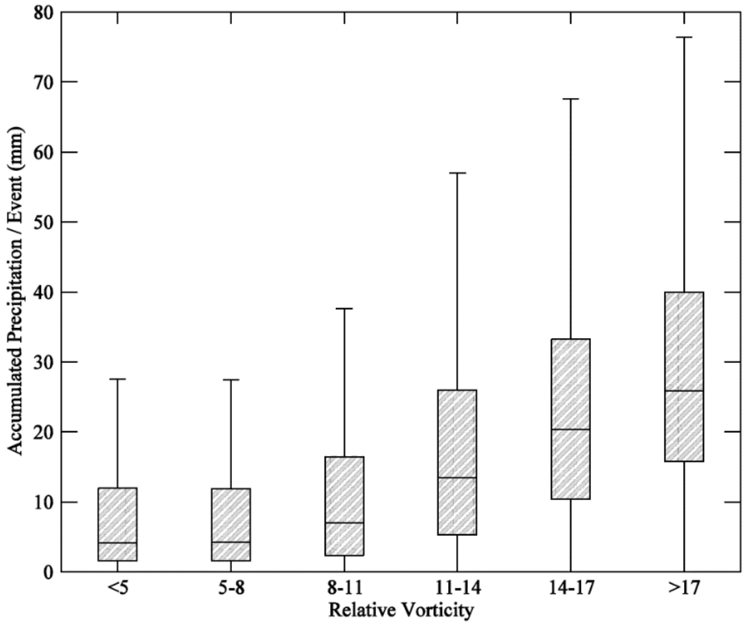

Figure 7 Boxplot illustrating the cumulative precipitation (mm) along the tracks of all identified Cut-off Lows with respect to intensity range. Intensity is measured in terms of the maximum ξ_{300} scale by -1.0 x 10^{-5} s^{-1}. The number of identified Cut-off Lows for each intensity range is: 1,084 (<5.0); 3,738 (5.0-8.0); 5,360 (8-11); 4,856 (11.0-14.0); 2,693 (14.0-17.0); 955 (>17.0). The top and bottom lines of the light gray box denote the 75th and 25th percentiles, respectively; the black line in the box centre represents the 50th percentile (median); the top and bottom whiskers indicate the upper and lower extremes, respectively.

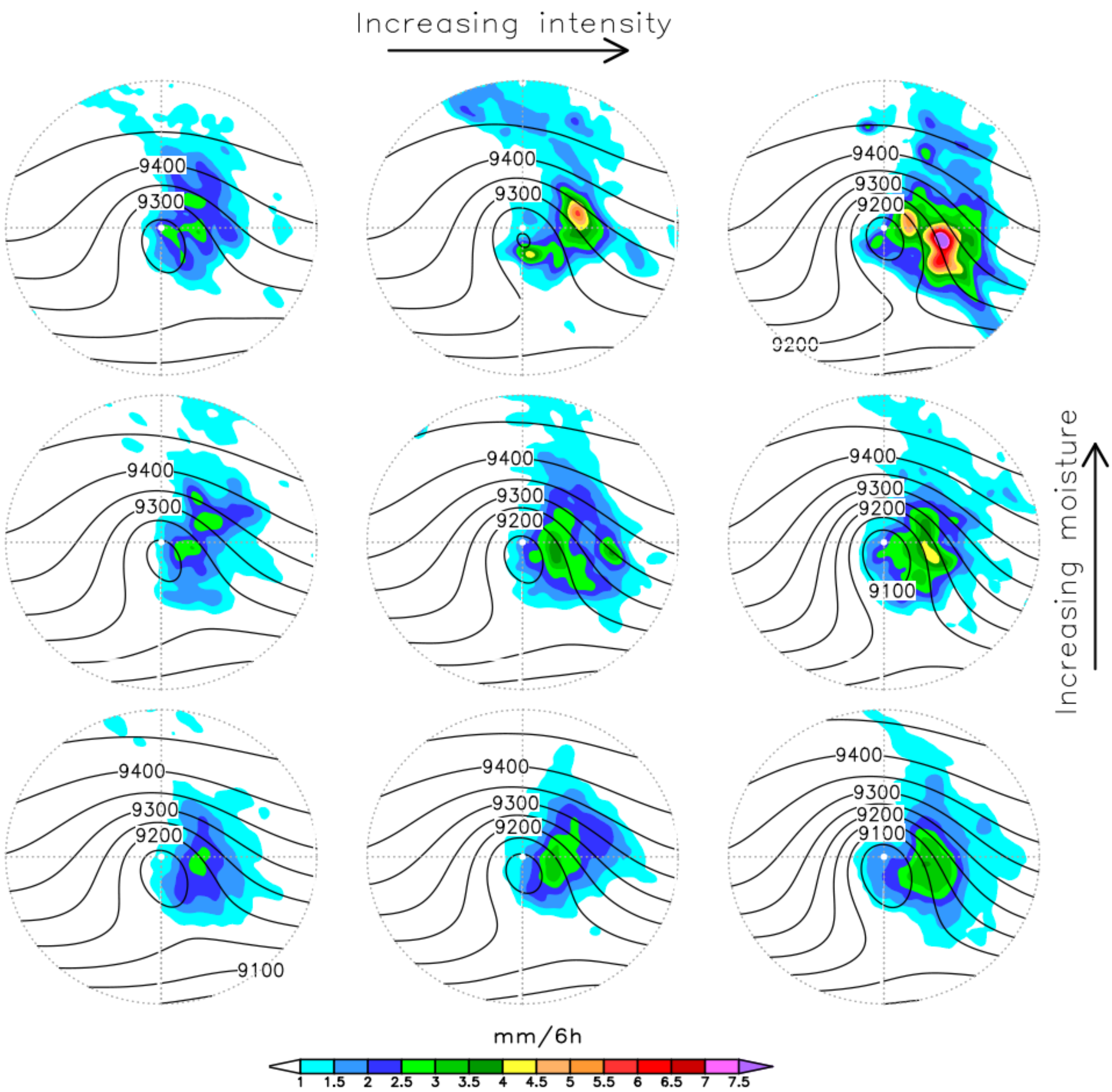

Figure 8 Composites of Southern Hemisphere Cut-off Lows for precipitation as a function of intensity and moisture. Plots are precipitation in mm/6h (shaded) and Z_{300} in gpm (solid line). Composites are determined as a function of intensity (ξ_{300}, increasing from left to right) and moisture (total column water, increasing from bottom to top). The two fields are calculated using the ξ_{300} Cut-off Lows for the time of ξ_{300} minimum. Precipitation is calculated using area average within 5° spherical arc radius centred on the ξ_{300} minimum. The categories are: [intensity]: 9.3-10.5, 10.5-12.0, 12.0-19.0 s^{-1} (scaled by -1 x 10^{-5}); and [moisture]: 27.6-30.8, 30.8-34.7, 34.7-40.0 kg/m^2. The number of Cut-off Lows used in each nine composite and the corresponding area-

Figure 8 (continuation) average accumulated precipitation (mm) over the whole lifecycle are, respectively: top left (126; 13.8), top centre (73; 15.6), top right (49; 20.1), middle left (145; 15.0), middle centre (135; 18.7), middle right (91; 21.6), bottom left (207; 18.7), bottom centre (182; 20.9), bottom right (169; 26.1).

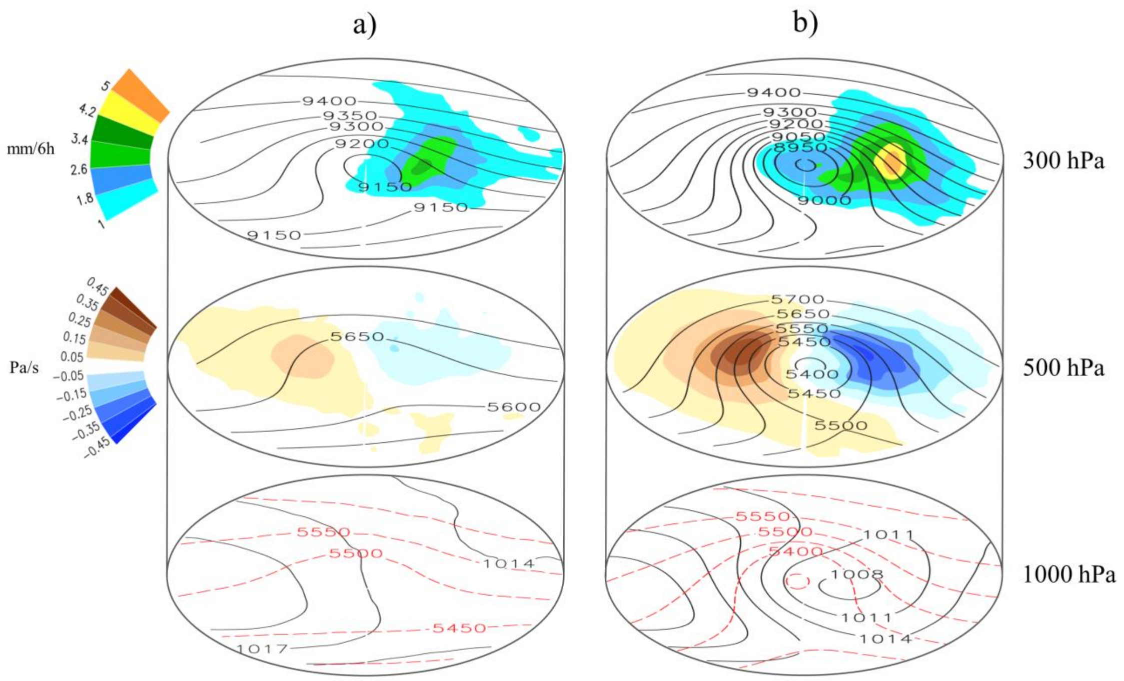

Figure 9 A three-dimensional schematic view of the a) average Cut-off Lows and the b) strongest Cut-off Lows. Fields are: [top]: 300-hPa geopotential height (black line) in gpm and precipitation (shaded) in mm/6h; [middle]: 500-hPa geopotential height (black line) in gpm and 500-hPa vertical velocity (shaded) in Pa s^{-1}; [bottom]: mean sea level pressure (black line) in hPa and 1000-500 hPa thickness (red dashed line) in gpm. Analysis performed using the Cut-off Lows that match between the ξ_{300} and Z'_{300}.

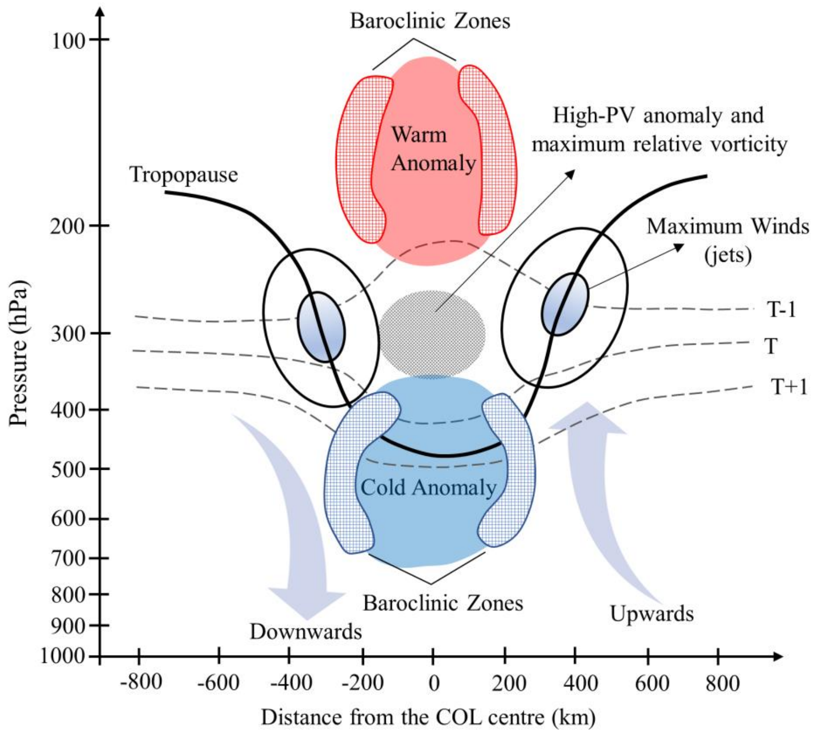

Figure 10 Schematic of typical structural features during the mature stage of a Cut-off Low (west-east cross-section). The thick black line represents the dynamical tropopause (2.0 PVU surface), gray dashed line indicates temperature, wide arrows indicate the vertical motions, the blue and red colour regions mean the cold and warm anomalies respectively with their associated baroclinic zones (in texture). The gray texture indicates the high-PV anomaly and maximum magnitude of relative vorticity. Adapted from Llasat et al. (2006).